

# Mesomorphic properties of chiral nematic star-shaped liquid crystals containing melitose as cores

Mei Tian<sup>a</sup>, Bao-Yan Zhang<sup>a,\*</sup>, Yue-Hua Cong<sup>b</sup>, Xiao-Zhi He<sup>a</sup>, Bing Zhang<sup>a</sup>

<sup>a</sup> Centre for Molecular Science and Engineering, Northeastern University, Shen-yang 110004, People's Republic of China

<sup>b</sup> PolyTherics Ltd., The London Bioscience Innovation Centre, 2 Royal College Street, London NW1 0TU, United Kingdom

## ARTICLE INFO

### Article history:

Received 10 June 2009

Received in revised form 21 August 2009

Accepted 26 August 2009

Available online 31 August 2009

### Keywords:

Star-shaped liquid crystal

Melitose

Chiral nematic

## ABSTRACT

Three star-shaped compounds (SSCs, **c1–c3**), are synthesized by using melitose as the chiral core and monacid (**b1**, **b2** and **b3**) as side arms, respectively. The side arms (**b1**, **b2** and **b3**), in which terminal chains are different, are introduced into the hydroxyl groups of melitose by esterification, respectively. The chemical structures of **c1–c3** are confirmed by FT-IR and <sup>1</sup>H NMR. The roles played by the chiral core and the side arms in the mesomorphic properties of the SSCs are studied. **b1** is not a liquid crystal (LC), while **b2** and **b3** are nematic LCs. **c1** is not a LC, while **c2** and **c3** are star-shaped LCs (SSLCs) and exhibit fingerprint texture of chiral nematic. **c1**, **c2** and **c3** are all levo-SSCs, which are different from their parent cores. The absolute value of their specific rotation increases with the increase of the terminal chain length of the side arms. The melting temperature of SSCs decreases with the increase of the terminal chain length of the side arms. For **c2–c3**, their mesomorphic region increases with the increase of the terminal chain length of the side arms. The results suggest that the LC properties of the side arms play an important role in inducing LC properties of the SSCs and the chiral core induces the chiral nematic of SSLCs, which contain the nematic LCs as the side arms.

© 2009 Elsevier B.V. All rights reserved.

## 1. Introduction

During the last decade, cholesteric liquid crystals (ChLCs) have attracted considerable interest for their unique optical properties, such as thermochromism, selective reflection of light and circular dichroism and advanced applications for instance nonlinear optical devices, full-color thermal imaging, and organic pigment [1–11]. ChLCs usually contain cholesterol derivatives LCs and chiral nematic (N<sup>\*</sup>) LCs. As one kind of unconventional LCs, star-shaped LC (SSLC) usually has a core and symmetric or non-symmetric mesogens as the side arms [12–38]. Derivatives of benzene and condensed aromatic rings are often taken as cores of SSLCs. The SSLCs usually exhibit thermotropic or lyotropic LC properties [39]. The common mesophase of SSLCs is columnar phase. To the best of our knowledge, cholesteric SSLCs have been few synthesized and sugars have seldom been taken as cores in synthesizing SSLCs. Yao [12], Saez [17] and Zhang [37] introduced cholesteric mesomorphic arms into flexible cores and obtained the cholesteric SSLCs. In these conditions, the cholesteric mesomorphic phases of the SSLCs were induced mainly by cholesteric mesomorphic arms. To study the effect of side arms on inducing LC properties of SSC, non-LC arm (**b1**) and LC arms (**b2** and **b3**) are chosen to introduce into the core in this article. To study the effect of chiral core on inducing chole-

steric mesomorphic phase of SSLCs, nematic mesomorphic arms (**b2** and **b3**) and melitose are chosen to synthesize the SSLCs. Melitose has also a different name, namely raffinose. This sugar is known to be incorporated easily into lyotropic liquid crystals and is even known to help in cosmetic industry to stabilize a lamellar structure of a part of the skin. In the article, melitose is used as a flexible and chiral core. The influence of the chiral core and the side arms on the mesomorphic properties of the SSCs is carefully studied and discussed here.

## 2. Experimental procedures

### 2.1. Materials

P-alkoxybenzoxoy, hydroquinol, and anhydrous melitose were obtained from Beijing Chemical Industry Company (China). Hexanedioic acid, thionyl chloride, pyridine and tetrahydrofuran were bought from Shenyang Chemical Industry Company (China). DCC and DMAP were bought from Shanghai Chemical Industry Company (China). All solvents were purified by standard methods.

### 2.2. Measurement

FT-IR spectra were measured on a Spectrum One (B) spectrometer (Perkin-Elmer, Foster City, CA, USA). Proton nuclear magnetic

\* Corresponding author.

E-mail address: [baoyanzhang@hotmail.com](mailto:baoyanzhang@hotmail.com) (B.-Y. Zhang).

resonance ( $^1\text{H}$  NMR) spectra (300 MHz) were obtained with a Gemini 300 spectrometer (Varian Associates, Palo Alto, CA). The elemental analyses were carried out with Elementar Vario EL III (Elementar, Hanau, Germany). Phase-transition temperatures and thermodynamic parameters were determined with a DSC 204 (Netzsch, Wittelsbacherstr, Germany). The heating and cooling rates were  $10\text{ }^\circ\text{C min}^{-1}$  under nitrogen atmosphere. The reported thermal transition temperatures were collected during the first heating and cooling cycle. A DMRX POM instrument (Leica, Wetzlar, Germany) equipped with a THMSE-600 hot stage (Linkam, Surrey, England) was used under an atmosphere to observe the phase-transition temperatures and analyze the LC properties for the SSLCs through the observation of optical textures. XRD measurements were performed with nickel-filtered  $\text{Cu K}\alpha$  ( $\lambda = 1.52\text{ \AA}$ ) radiation with a DMAX-3A powder diffractometer (Rigaku, Tokyo, Japan). The optical activities for the SSCs were determined with a Perkin-Elmer Model 341 Polarimeter. All optical activity measurements of SSCs were carried out in tetrahydrofuran (THF) with 2 ml cuvette of 100 mm length using light of a Na-lamp at  $\lambda = 589\text{ nm}$ .

### 2.3. Synthesis

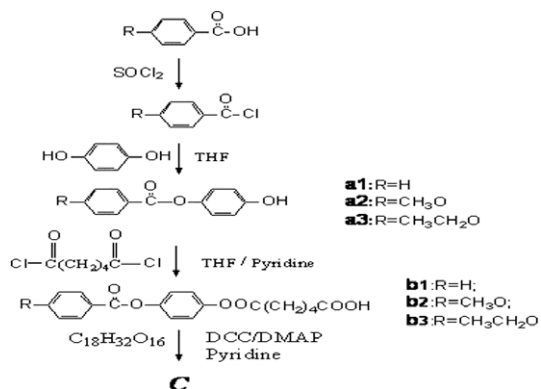
The synthetic route of side arms and SSCs are shown in Schemes 1 and 2, respectively.

#### 2.3.1. 6-(4-(alkoxybenzoyloxy)phenoxy)-6-oxohexanoic acid (**b1–b3**)

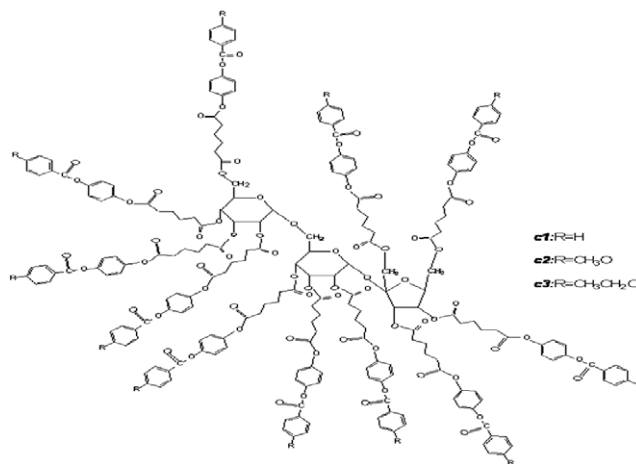
For the syntheses of 6-(4-benzoyloxy) phenoxy)-6-oxohexanoic acid (**b1**), 6-(4-(4-methoxybenzoyloxy) phenoxy)-6-oxohexanoic acid (**b2**) and 6-(4-(4-ethoxybenzoyloxy) phenoxy)-6-oxohexanoic acid (**b3**), the same methods are adopted. The synthesis of **b3** is given as an example.

The mixture of 4-ethoxybenzoic acid (16.6 g, 0.1 mol) and thionyl chloride (47.6 g, 0.4 mol) in a 250 ml round-bottom flask was stirred for 2 h at room temperature, and then heated to reflux at  $78\text{ }^\circ\text{C}$  for 4 h. The excess thionyl chloride was removed to give the corresponding acid chloride. The acid chloride (18.4 g, 0.1 mol) was dissolved in THF (20 ml). The solution was then added drop wise into the solution of hydroquinol (44 g, 0.4 mol) in 100 ml THF and 10 ml Pyridine under quick stirring. The reaction mixture refluxed for 18 h and poured into 1000 ml ice water and neutralized with dilute hydrochloric acid. The crude product was obtained by filtration and washed with hot water. The white powder **a3** was obtained by recrystallization from ethanol. Yield 46%.

Compound **a3** (25.8 g, 0.1 mol) was dissolved in the solution of THF (80 ml) and dry pyridine (10 ml). The resulted solution was then added drop wise to solution of hexanedioic chloride (36.6 g, 0.2 mol) in 50 ml THF. The reaction mixture refluxed for 15 h and poured into ice water. The crude product was obtained by filtration



Scheme 1. The syntheses of star-shaped compounds **c**.



Scheme 2. The structures of star-shaped compounds **c**.

and washed with water and cold ethanol. The white powder **b3** was obtained by recrystallization from ethanol. Yield 37%.

#### 2.3.2. Hende{6-(4-(alkoxybenzoyloxy) phenoxy)-6-oxohexanoic acid}melitose ester (**c1–c3**)

**c1–c3** are prepared by the same synthetic method. The synthesis of **c3** is given as an example. The anhydrous melitose (0.504 g, 1 mmol) solution in dry pyridine (20 ml) was added into the solution of **b3** (4.25 g, 11 mmol) in dry pyridine (60 ml) containing DCC (2.266 g, 11 mmol) and DMAP (0.366 g, 3 mmol). The reaction mixture was stirred for 72 h at room temperature and filtrated. The filtrate was poured into water and acidified with dilute hydrochloric acid. The crude product was obtained by filtration and washed with water to neutral pH. The white powder **c3** was obtained by recrystallization from ethanol.

**c1** Yield: 41%, m.p.  $169.0\text{ }^\circ\text{C}$ . Elemental analysis calculated for  $\text{C}_{227}\text{H}_{208}\text{O}_{71}$ : C, 66.96; H, 5.11%. Found: C, 66.76; H, 5.21%.

IR (KBr,  $\text{cm}^{-1}$ ): 2928, 2865 ( $-\text{CH}_2-$ ), 1752–1722 ( $\text{C}=\text{O}$ ), 1610, 1510 ( $-\text{Ar}$ ), 1251, 1046 ( $\text{C}-\text{O}-\text{C}$ ).

$^1\text{H}$  NMR ( $\text{CDCl}_3$ , TMS,  $\delta$ , ppm): 1.557–1.584 (m, 44H,  $-\text{CH}_2-$ ), 2.384–2.640 (m, 44H,  $-\text{CH}_2-$ ), 4.328–5.665 [m, 19H, pyranose - H (except H-1)], 5.862 (d, 1H,  $J = 5.4\text{ Hz}$ ), 6.683 (d, 1H,  $J = 2.8\text{ Hz}$ ), 7.115–7.139 (m, 22H, Ar-H), 7.203–7.226 (m, 22H, Ar-H), 7.369–7.381 (m, 33H, Ar-H), 8.139–8.161 (m, 22H, Ar-H).

**c2** Yield: 43%, m.p.  $150.4\text{ }^\circ\text{C}$ . Elemental analysis calculated for  $\text{C}_{238}\text{H}_{230}\text{O}_{82}$ : C, 64.94; H, 5.23%. Found: C, 64.58; H, 5.63%.

IR (KBr,  $\text{cm}^{-1}$ ): 2968, 2852 ( $-\text{CH}_3$ ,  $-\text{CH}_2-$ ), 1757–1728 ( $\text{C}=\text{O}$ ), 1610, 1506 ( $-\text{Ar}$ ), 1268, 1042 ( $\text{C}-\text{O}-\text{C}$ ).

$^1\text{H}$  NMR ( $\text{CDCl}_3$ , TMS,  $\delta$ , ppm): 1.780–1.802 (m, 44H,  $-\text{CH}_2-$ ), 2.429–2.464 (m, 22H,  $-\text{CH}_2-$ ), 2.572–2.596 (m, 22H,  $-\text{CH}_2-$ ), 3.746–3.801 (m, 33H,  $\text{CH}_3\text{O}-$ ), 4.335–5.676 [m, 19H, pyranose - H (except H-1)], 5.861 (d, 1H,  $J = 5.4\text{ Hz}$ ), 6.680 (d, 1H,  $J = 2.8\text{ Hz}$ ), 6.954–6.977 (m, 22H, Ar-H), 7.115–7.139 (m, 22H, Ar-H), 7.206–7.228 (m, 22H, Ar-H), 8.118–8.150 (m, 22H, Ar-H).

**c3** Yield: 48%, m.p.  $121.1\text{ }^\circ\text{C}$ . Elemental analysis calculated for  $\text{C}_{249}\text{H}_{252}\text{O}_{82}$ : C, 65.64; H, 5.54%. Found: C, 65.25; H, 5.71%.

IR (KBr,  $\text{cm}^{-1}$ ): 2967, 2863 ( $-\text{CH}_3$ ,  $-\text{CH}_2-$ ), 1760–1730 ( $\text{C}=\text{O}$ ), 1608, 1510 ( $-\text{Ar}$ ), 1276, 1046 ( $\text{C}-\text{O}-\text{C}$ ).

$^1\text{H}$  NMR ( $\text{CDCl}_3$ , TMS,  $\delta$ , ppm): 1.441–1.477 (m, 33H,  $-\text{CH}_3$ ), 1.795–1.815 (m, 44H,  $-\text{CH}_2-$ ), 2.426–2.461 (m, 22H,  $-\text{CH}_2-$ ), 2.588–2.623 (m, 22H,  $-\text{CH}_2-$ ), 4.099–4.151 (m, 22H,  $-\text{CH}_2\text{O}-$ ), 4.331–5.680 [m, 19H, pyranose - H (except H-1)], 5.864 (d, 1H,  $J = 5.4\text{ Hz}$ ), 6.678 (d, 1H,  $J = 2.8\text{ Hz}$ ), 6.953–6.975 (m, 22H, Ar-H), 7, 118–7.140 (m, 22H, Ar-H), 7.200–7.223 (m, 22H, Ar-H), 8.117–8.150 (m, 22H, Ar-H).

### 3. Results and discussion

#### 3.1. Synthesis

The synthetic routes for the side arms and SSCs are shown in Schemes 1 and 2. Their structural characterizations are in good agreement with the prediction. The side arms (**b1**, **b2** and **b3**) are synthesized through the reaction of compounds **a** and hexanedioic chloride in THF and pyridine. IR characteristic bands of **b1–b3** between 4000 and 400  $\text{cm}^{-1}$  are as follows, 3260–2500 ( $-\text{OH}$  in carboxylic acid), 1760–1713 ( $\text{C}=\text{O}$  in aromatic ester mode), 1708 ( $\text{C}=\text{O}$  in carboxylic acid mode), 1607, 1509, 1467, 731 and 691 (characteristic bands of aromatic ring), 1260, 1078 ( $\text{C}-\text{O}$  stretching).  $^1\text{H}$  NMR spectra of **b1–b3** show a series of multiple peaks at 1.441, 1.557–4.100 and 6.902–8.131 corresponding to methyl, methylene and aromatic, respectively.

For **c1–c3**, the disappearance of the  $-\text{OH}$  and  $-\text{COOH}$  characteristic bands at 3260–2500 and 1708  $\text{cm}^{-1}$  indicates that side arms **b1–b3** have been successfully incorporated into melitose. For **c1–c3**, their characteristic bands are as follows: 2968–2852  $\text{cm}^{-1}$  ( $-\text{CH}_3$ ,  $-\text{CH}_2-$ ), 1760–1722  $\text{cm}^{-1}$  ( $\text{C}=\text{O}$  stretching in different kinds of ester modes), 1610, 1506  $\text{cm}^{-1}$  ( $\text{Ar}-$ ).  $^1\text{H}$  NMR spectra of **c1–c3** show peaks at 1.441–1.815, 2.384–4.151, 4.328–6.683 and 6.953–8.161 corresponding to methyl, methylene, sugar ring and aromatic, respectively. The results of FT-IR,  $^1\text{H}$  NMR spectroscopy and element analysis indicate that the target compounds **c1**, **c2** and **c3** are obtained.

#### 3.2. Optical rotation

Melitose is optically active in water solution and the specific rotation (SROT) of melitose is  $+105^\circ$ . The SSCs (in THF,  $c = 0.8 \text{ g/L}$ ) exhibit optical activity, too. The SROT of **c1**, **c2** and **c3** are  $-23.65^\circ$ ,  $-34.85^\circ$  and  $-46.92^\circ$ , respectively (see Table 1). It is obvious that the chiral core plays an important role in the optical activity of the SSCs. However, the SROT of the SSCs show contrary handedness to their parent cores. Generally, solvent, temperature, chain length and substituent play an important effect on handedness of the cholesteric liquid crystals [40,41]. In this study, the results suggest that the long side arms play an important effect on the change of the behavior of SROT for SSCs. For **c1–c3**, the absolute value of SROT increases with the increase of terminal chain length in the side arms. It indicates that the longer the terminal chain is the more freedom the chain structure has and the higher the SROT value is.

#### 3.3. Mesomorphic properties

The thermal properties and phase behavior of side arms and SSCs are investigated with DSC. Their phase-transition temperatures and corresponding enthalpy changes, obtained on the first heating and cooling cycle, are summarized in Table 2, and the DSC curves of SSCs are presented in Fig. 1.

**b1** only shows a melting transition and a crystalline transition at 205.4  $^\circ\text{C}$  and 183.1  $^\circ\text{C}$  on heating and cooling cycle, respectively. **b2** shows a melting transition at 138.0  $^\circ\text{C}$  on heating cycle, and a

**Table 1**  
Inventory ratio, specific rotation and yield of star-shaped compounds **c1–c3**.

Sample	<b>b1</b> (mmol)	<b>b2</b> (mmol)	<b>b3</b> (mmol)	$\text{ME}^{\text{a}}$ (mmol)	$\alpha_{589}^{20}$ ( $^\circ$ )	Yield (%)
<b>c1</b>	11.00	–	–	1.00	$-23.65$	41
<b>c2</b>	–	11.00	–	1.00	$-34.85$	43
<b>c3</b>	–	–	11.00	1.00	$-46.92$	48

<sup>a</sup> Melitose.

**Table 2**

Mesomorphic properties of side arms and star-shaped compounds.

Sample	Transition temperature $^\circ\text{C}$ (corresponding enthalpy changes in $\text{J g}^{-1}$ )		$\Delta T^{\text{e}}$ ( $^\circ\text{C}$ )	LC Phase
	Heating	Cooling		
<b>b1</b>	Cr <sup>a</sup> 205.4 (68.5) I <sup>b</sup>	–	–	–
	Cr 181.3 ( $-65.6$ ) I	–	–	–
<b>b2</b>	Cr 138.0 (10.74) I	–	–	N <sup>c</sup>
	Cr 72.0 ( $-8.95$ ) N 137.2 ( $-0.69$ ) I	–	65.2	–
<b>b3</b>	Cr 122.4 (44.7) N 140.5 (2.71) I	–	18.1	N
	Cr 72.4 ( $-13.95$ ) N 140.0 ( $-0.59$ ) I	–	67.6	–
<b>c1</b>	Cr 169.0 (73.64) I	–	–	–
	Cr 139.1 ( $-56.08$ ) I	–	–	–
<b>c2</b>	Cr 150.4 (18.47) N <sup>d</sup> 193.9 (4.18) I	–	43.5	N <sup>d</sup>
	Cr 99.6 ( $-1.196$ ) N <sup>d</sup> 192.4 ( $-0.49$ ) I	–	92.8	–
<b>c3</b>	Cr 121.1 (45.5) N <sup>d</sup> 189.1 (2.406) I	–	68.0	N <sup>d</sup>
	Cr 64.5 ( $-13.1$ ) N <sup>d</sup> 191.5 ( $-1.158$ ) I	–	120.0	–

<sup>a</sup> Crystalline.

<sup>b</sup> Isotropic.

<sup>c</sup> Nematic.

<sup>d</sup> Chiral nematic.

<sup>e</sup> Mesophase temperature ranges.

isotropy–LC transition at 137.2  $^\circ\text{C}$  and a LC–crystal transition at 72.0  $^\circ\text{C}$  on cooling cycle. **b2** exhibits schlieren texture on cooling cycle and its mesomorphic region ( $\Delta T_2$ ) is 65.2  $^\circ\text{C}$ . **b3** shows a melting transition at 122.4  $^\circ\text{C}$ , a clearing transition at 140.5  $^\circ\text{C}$  and the mesomorphic region ( $\Delta T_1$ ) about 18.1  $^\circ\text{C}$  on heating cycle. While on cooling cycle, the isotropy–LC transition and LC–crystal transition was at 140.0  $^\circ\text{C}$  and 72.0  $^\circ\text{C}$ , respectively. The mesomorphic region ( $\Delta T_2$ ) was about 67.6  $^\circ\text{C}$ . **b3** exhibits schlieren texture and thread texture on heating and cooling cycle.

**c1** does not exhibit any textures and only shows melting and crystal transitions on heating and cooling cycle, respectively. **c2** and **c3** show melting transitions at 150.4 and 121.1  $^\circ\text{C}$ , clearing transitions at 193.9 and 189.1  $^\circ\text{C}$ , the mesomorphic regions ( $\Delta T_1$ ) about 43.5 and 68.0  $^\circ\text{C}$  on heating cycle. On cooling cycle, **c2** and **c3** show isotropy–LC transitions at 192.4 and 191.5  $^\circ\text{C}$ , LC–crystal transitions at 99.6 and 64.5  $^\circ\text{C}$ , the mesomorphic regions ( $\Delta T_2$ ) about 92.8 and 120.0  $^\circ\text{C}$ , respectively.

The structure of side arms plays an important role in the properties of SSCs. Only when the side arms show LC properties, the SSCs exhibit LC properties. For **c1–c3**, with the increase of terminal chain of side arms, the melting temperature decreases, and for **c2** and **c3**, the mesomorphic region widens. The increasing terminal chain acts as the plasticizer and makes the melting temperature decrease.

The chiral core plays an important role in the mesomorphic type of **c2** and **c3**. Different from their side arms, **c2** and **c3** exhibit fingerprint texture of chiral nematic (N<sup>d</sup>). For **c3**, when it was heated at 150  $^\circ\text{C}$ , the sample melted and fingerprint texture appeared. The texture disappeared at 193.4  $^\circ\text{C}$ . When the isotropic state was cooled to 192.4  $^\circ\text{C}$ , cholesteric droplet, in which shown fingerprint texture, separated from the isotropic melt as shown in Fig. 2(a), and gradually coalesced and the typical fingerprint texture appeared as shown in Fig. 2(b). The sample exhibited fingerprint texture until crystallization. **c2** exhibited fingerprint texture on heating and cooling cycle, too (see Fig. 2c). Fingerprint texture is a typical texture of chiral nematic phase. For fingerprint texture, the twist axis lie in the plane of the substrate, within the substrate plane there is no preferred direction, and thus the direction of the twist axis is allowed to vary smoothly over macroscopic

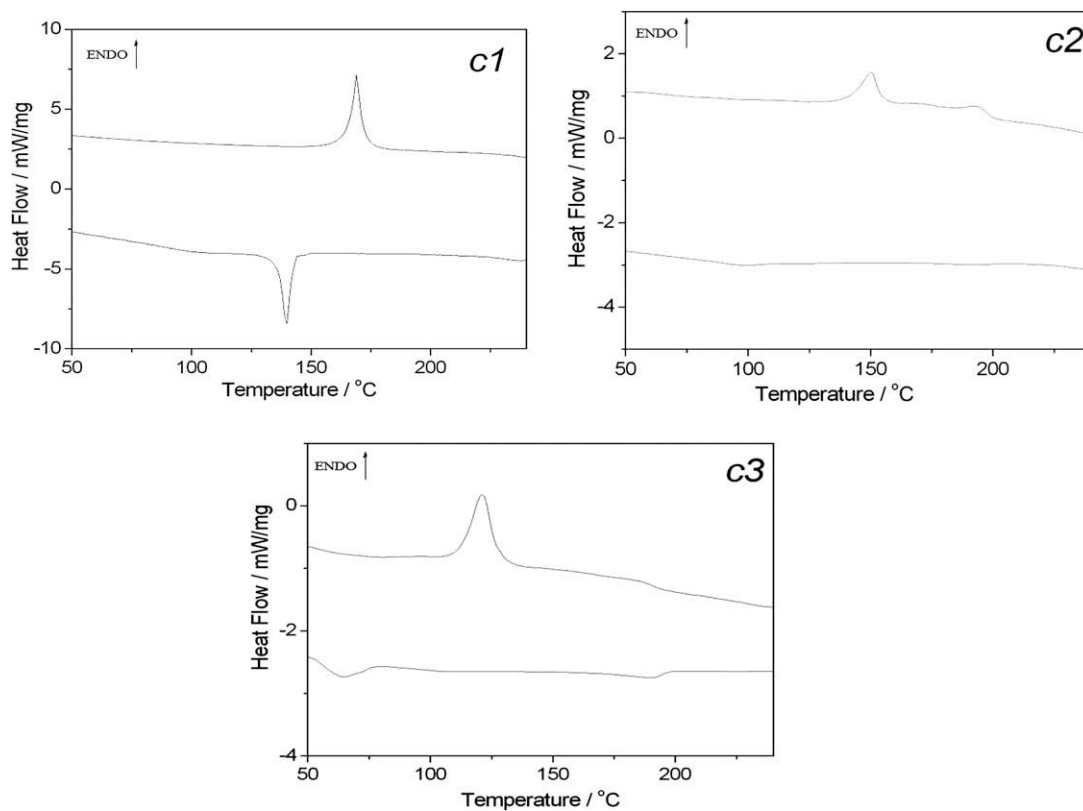


Fig. 1. DSC thermograms of star-shaped compounds **c1**–**c3**.

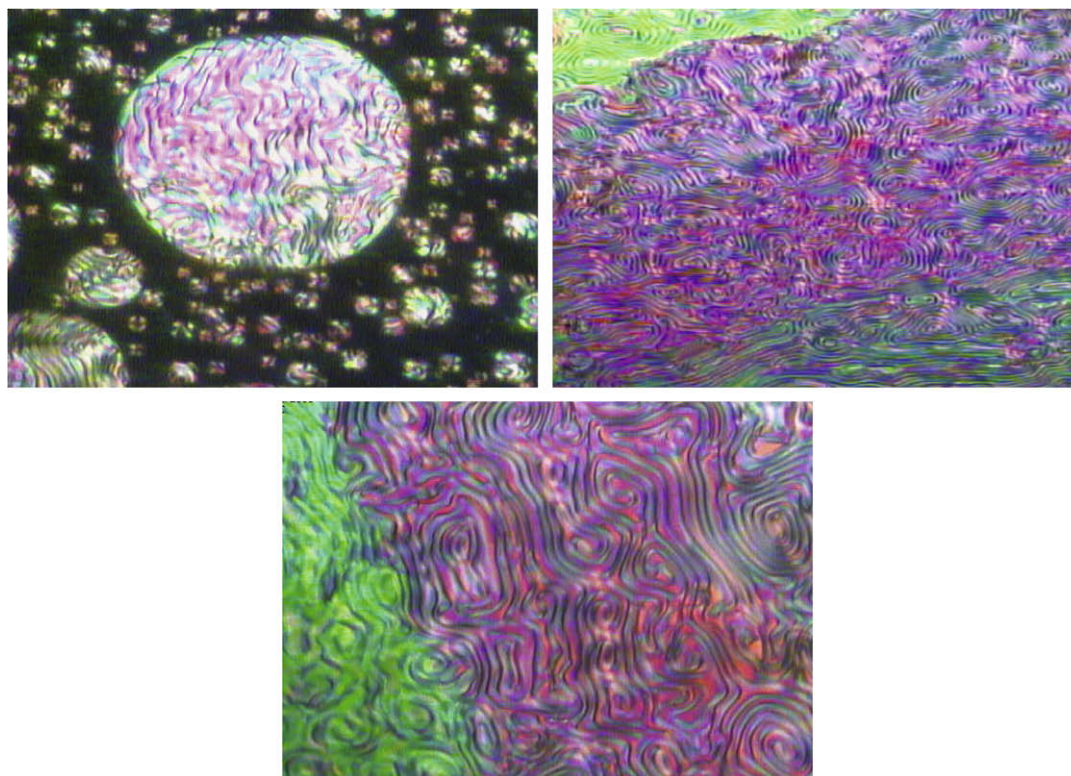


Fig. 2. Optical polarizing micrographs for **c2** and **c3**: (a) droplet texture of **c3** on cooling to 187.0 °C (500×). (b) Fingerprint texture of **c3** on cooling to 156.0 °C (200×). (c) Fingerprint texture of **c2** on cooling to 145.0 °C (500×).

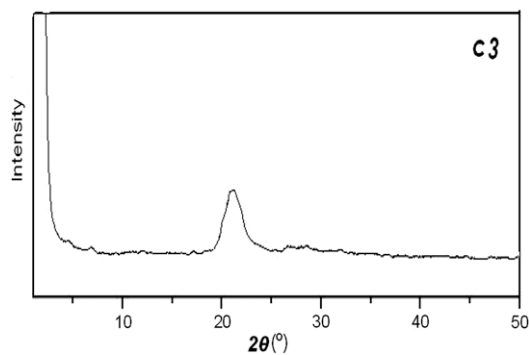


Fig. 3. X-ray diffraction pattern of **c3**.

distances. The varying director field leads to an equidistant pattern of dark lines, which is called a fingerprint texture. Dark stripes appear, whenever the local director is oriented along the direction of light propagation, i.e. at vanishing birefringence [42].

XRD studies are carried out to obtain more detailed information on the LC phase structures and types. In general, a sharp and strong peak at low angle ( $1^\circ < 2\theta < 4^\circ$ ) in the small angle X-ray scattering (SAXS) curve and a broad peak associated with lateral packing at  $2\theta \approx 20^\circ$  in the wide angle X-ray diffraction (WAXD) curve can be observed for smectic structure. For the nematic structure, no peaks appear in SAXS curve, but in the WAXD, a broad peak at  $2\theta \approx 20^\circ$  can also be observed. For cholesteric structure, no peak appears in SAXS, too. However, a broad peak occurs at  $2\theta \approx 16\text{--}18^\circ$  or  $20^\circ$ . The quenched samples of **c2** and **c3** are studied by SAXS and WAXS. In this study, a diffuse peak at about  $2\theta = 21^\circ$  ( $d = 4.17 \text{ \AA}$ , calculated by  $\lambda = 2d\sin\theta$ ) in WAXD curves, are observed for **c2** and **c3**, respectively, and there is no sharp peak at low angles region. The representative X-ray of **c3** is shown in Fig. 3. The XRD data are consistent with their optical textures, which suggest that **c2** and **c3** are  $N^+$  SSLCs. The results suggest that melitose plays an important role in inducing the  $N^+$  phase.

#### 4. Conclusions

Three SSCs are prepared from the melitose core and the side arms with different terminal chain (**b1–b3**). They exhibit levo specific rotation and the absolute value of specific rotation increases with the increase of terminal chain length in the side arms.

The appearance of LC properties of SSCs depends on the properties of side arms. Only when the side arm is a LC, the SSCs display LC properties. **b1** and **c1** are non-LC compounds. **b2**, **c2** and **b3**, **c3** exhibit mesomorphic properties. The length of terminal chain of side arms also affects the phase transition temperature of SSCs. For **c1–c3**, with the increase of terminal chain, the melting temperature decreases. For **c2** and **c3**, with the increase of terminal chain, the mesomorphic region widens. They exhibit the typical fingerprint texture of  $N^+$  different from their nematic side arms. The XRD data are consistent with their optical textures. The results indicate that melitose core could induce  $N^+$  of SSLCs, which containing nematic side arms.

#### Acknowledgments

The authors are grateful to National Natural Science Fundamental Committee of China and HI-Tech Research and development programmer (863) of China, the commission for science, technology and industry for national defense (DBDX2008038) of china and the Science and Technology Department of Liaoning Province financial support of this work.

#### References

- [1] J.P. Lin, D.F. Zhou, Chem. Res. Chin. Univ. 16 (2000) 169.
- [2] H. Kosho, Y. Tanaka, T. Ichizuka, Polym. J. 31 (1999) 199.
- [3] S.M. Yu, V.P. Conticello, G.H. Zhang, Nature 389 (1997) 167.
- [4] D.M. Anne, S. Etienne, Macromol. Chem. 193 (1992) 3031.
- [5] T.T. Chong, T. Heidelberg, R. Hashim, S. Gary, Liq. Cryst. 34 (2007) 267.
- [6] G. John, H. Minamikawa, M. Masuda, T. Shimizu, Liq. Cryst. 30 (2003) 747.
- [7] R. Judele, S. Laschat, A. Baro, M. Nimtz, Tetrahedron 62 (2006) 9681.
- [8] H. Meier, M. Lehmann, Tetrahedron 60 (2004) 6881.
- [9] H. Goto, X. Dai, H. Narihiro, K. Akagi, Macromolecules 37 (2004) 2353.
- [10] J. Liu, Q.Z. Zhang, J.Z. Zhang, Mater. Lett. 59 (2005) 2531.
- [11] V. Vill, T. Bocker, J. Thiem, F. Fischer, Liq. Cryst. 33 (2006) 1353.
- [12] D.S. Yao, B.Y. Zhang, W.W. Zhang, M. Tian, J. Mol. Struct. 881 (2008) 83.
- [13] J. Brettar, T. Bürgi, B. Donnio, D. Guillon, R. Klappert, T. Scharf, R. Deschenaux, Adv. Funct. Mater. 16 (2006) 260.
- [14] A.S. Abd-El-Aziz, S.A. Carruthers, P.M. Aguiar, S. Kroeker, J. Inorg. Organomet. Polym. Mater. 15 (2005) 349.
- [15] S. Abraham, S. Paul, G. Narayan, S.K. Prasad, D.S.S. Rao, N. Jayaraman, S. Das, Adv. Funct. Mater. 15 (2005) 1579.
- [16] N. Tamaoki, Y. Aoki, M. Moriyama, M. Kidowaki, Chem. Mater. 15 (2003) 719.
- [17] I.M. Saez, J.W. Goodby, Chem. Eur. J. 9 (2003) 4869.
- [18] M. Shi, H. Zhang, J. Chen, X. Wan, Q. Zhou, Polym. Bull. 52 (2004) 401.
- [19] M. Lehmann, R.I. Gearba, M.H.J. Koch, D.A. Ivanov, Chem. Mater. 16 (2004) 374.
- [20] M. Lehmann, M. Jahr, F.C. Grozema, R.D. Abellon, L.D.A. Siebbeles, M. Muller, Adv. Mater. 20 (2008) 1.
- [21] X.Z. Wang, H.L. Zhang, D.C. Shi, J.F. Chen, et al., Eur. Polym. J. 41 (2005) 933.
- [22] H. Bisoyi, S. Kumar, Tetrahedron Lett. 49 (2008) 3628.
- [23] B.Y. Zhang, D.S. Yao, F.B. Meng, Y.H. Li, J. Mol. Struct. 741 (2005) 135.
- [24] K.I. Suresh, J.R. Tamboli, B.S. Rao, S. Verma, G. Unnikrishnan, Polym. Adv. Technol. 19 (2008) 1323.
- [25] C. Pugh, A.M. Kasko, S.R. Grunwald, J. Polym. Sci. Part A: Polym. Chem. 46 (2008) 4363.
- [26] J.P. Majoral, A.M. Caminade, Chem. Rev. 99 (1999) 845.
- [27] M. Lehmann, M. Jahr, E. Donnio, R. Graf, S. Gemming, I. Popov, Chem. Eur. J. 14 (2008) 3562.
- [28] D.S. Yao, B.Y. Zhang, Y.H. Li, Tetrahedron Lett. 45 (2004) 8953.
- [29] B.G. Kim, S. Kim, S.Y. Park, Tetrahedron Lett. 42 (2001) 2697.
- [30] C. Galliot, D. Prevote, A.M. Caminade, J.P. Majoral, J. Am. Chem. Soc. 117 (1995) 5470.
- [31] L.L. Lai, C.H. Lee, L.Y. Wang, K.L. Cheng, H.F. Hsu, J. Org. Chem. 73 (2008) 485.
- [32] W. Mormann, C. Kuckertz, Macromol. Symp. 181 (2002) 113.
- [33] A. Zelcer, B. Donnio, C. Bourgoigne, F.D. Cukiernik, D. Guillon, Chem. Mater. 19 (2007) 1992.
- [34] J. Xu, T.C. Ling, C. He, J. Polym. Sci. Part A: Polym. Chem. 46 (2008) 4691.
- [35] A. Bubnov, V. Hamplov, M. Kaspar, A. Vajda, M. Stojanovic, D.Z. Obadovic, N. Eber, K. Fodor-Csorba, J. Therm. Anal. Cal. 90 (2007) 431.
- [36] C. Galliot, C. Larre, A.M. Caminade, J.P. Majoral, Science 277 (1997) 1981.
- [37] B.Y. Zhang, W.Q. Xiao, Y.H. Cong, et al., Liq. Cryst. 34 (2007) 1129.
- [38] M. Lehmann, Chem. Eur. J. 15 (2009) 3638.
- [39] J. Barbera, A.C. Garces, N. Jayaraman, A. Omenat, J.L. Serrano, J.F. Stoddart, Adv. Mater. 13 (2001) 175.
- [40] M.M. Green, K.S. Cheon, S.Y. Yang, J.W. Park, S. Swansburg, W.H. Liu, Acc. Chem. Res. 34 (2001) 672.
- [41] R. Nomura, Y. Fukushima, H. Nakako, T.J. Masuda, Am. Chem. Soc. 122 (2000) 8830.
- [42] I. Dierking, In Die Deutsche Bibliothek, Textures of Liquid Crystal, WILEY-VCH Verlag, Weinheim, 2003 (Chapter 5).